The Semidiurnal Variation in GPS-derived Zenith Neutral Delay

T. E. Humphreys

Sibley School of Mechanical and Aerospace Engineering, Cornell University, Ithaca, New York, USA

M. C. Kelley, N. Huber, and P. M. Kintner, Jr.

School of Electrical and Computer Engineering, Cornell University, Ithaca, New York, USA

Zenith neutral delay (ZND) estimates derived from ground-based GPS receivers exhibit variations at harmonics of the solar day. The aim of this work is to characterize the semidiurnal (S_2) variation and determine its probable origin. Data from 100 GPS sites are compared with surface pressure measurements to reveal close agreement between the estimated ZND S_2 variation and the S_2 surface pressure tide. Error analysis suggests that the S_2 variation in ZND estimates is not due primarily to orbit, solid earth, or Earth orientation modeling errors. Atmospheric loading and mapping function errors are each expected to contribute less than 11% to the estimated ZND S_2 amplitude. Local incongruities reflect the influence of water vapor or site-dependent errors.

1. Introduction

Since 1998 the International GPS Service (IGS) has included an estimated zenith neutral delay (ZND) (sometimes called tropospheric delay) among its official products. The ZND measures the amount by which the neutral atmosphere delays a GPS signal in excess of the free-space delay. ZND is conventionally measured in meters, with a nominal value of 2.4 m at sea level. Current ZND accuracy is about 4 mm [*Byun et al.*, 2005].

Spectral analysis of IGS ZND data reveals mm-level variations at harmonics of the solar day and at the lunar tidal frequency. An obvious explanation is that these variations reflect the regular tides induced on the atmosphere by solar and lunar thermal and gravitational excitation. Indeed, *Dai et al.* [2002] showed that a solar diurnal (S_1) variation in the wet component of GPS-derived ZND agrees roughly with that in microwave radiometer (MWR) and radiosonde measurements. However, *Humphreys et al.* [2004] showed that the amplitude of the lunar tide in IGS ZND data prior to 2000 is drastically reduced in post-2000 data, and that high-frequency solar harmonics extend well beyond S_6, contrary to the behavior of the surface pressure tides. Such results encourage careful scrutiny of the periodic variations in IGS ZND data if these are to be accepted as manifestations of actual atmospheric tides. Moreover, a close examination of the variations in GPS-derived ZND will be useful for detecting persistent periodic errors in the ZND record.

The S_2 variation in IGS ZND data will be the focus of this study. The approach taken will be to compare its global phase and amplitude distribution with that of the semidiurnal surface pressure tide, $S_2(p)$. With long wavelengths excited by ozone and water vapor absorption of solar radiation, the 12-hour $S_2(p)$ tide is characterized by a strong, zonally homogeneous surface pressure variation with tidal maximum occurring about 2 hours before local noon and midnight [*Chapman and Lindzen*, 1970; *Dai and Wang*, 1999; *Ray*, 2001]. A strong correlation between the global distribution of the two signals will provide evidence for the authenticity of the S_2 variation in IGS ZND estimates. Precision and likely errors will also be considered.

0094-8276/05/$5.00

2. Models, Data, and Analysis Technique

ZND is the integrated refractivity along a vertical path through the neutral atmosphere:

$$\tau^z = ct^z = 10^{-6} \int_0^\infty N(z) dz \tag{1}$$

where τ^z is ZND measured in units of distance, c is the speed of light in a vacuum, and t^z is the delay measured in units of time. Neutral atmosphere refractivity N is approximately related to the total mass density of moist air ρ (kg m^{-3}), temperature T (K), and partial pressure of water vapor e (mb) by the relation [*Davis et al.*, 1985]

$$N = 222.76\rho + (17 \pm 10)\frac{e}{T} Z_w^{-1} + 377600 \frac{e}{T^2} Z_w^{-1} \tag{2}$$

Here, Z_w is a factor near unity that accounts for the small departure of moist air from an ideal gas. The integral of the first term in Eq. (2) is designated the hydrostatic component, τ_h^z; the integral of the remaining two terms is the wet component, τ_w^z. Thus $\tau^z = \tau_h^z + \tau_w^z$.

The hydrostatic component dominates τ^z, accounting for roughly 90% of the total delay. It follows that τ^z is strongly correlated with surface pressure p_0. Disregarding the change in the acceleration of gravity g with height, the hydrostatic approximation $dp = -g\rho\, dz$ relates τ_h^z to p_0 by $\tau_h^z = (2.28 \text{ mm/mb}) p_0$. *Davis et al.* [1985] note that this scale factor varies less than 1% under extreme weather conditions. Assuming a typical 1-mb semidiurnal surface pressure tide $S_2(p)$, this scale factor predicts a semidiurnal ZND variation $S_2(\tau^z)$ with an amplitude of 2.28 mm. Thus, it is unsurprising to note variations in IGS ZND data at frequencies corresponding to the atmospheric tides (Fig. 1, left panel). Peaks at S_1 to S_6 are visible as well as a peak at the lunar tidal frequency, L_2 (nearly coincident with S_2). This paper will focus only on S_2, which, as observed in the IGS ZND data, will be denoted $S_2(\tilde{\tau}^z)$ to distinguish it from the error-free $S_2(\tau^z)$ variation. This is done to concede the possibility that the observed variations in IGS ZND data are due to causes other than actual tides in τ^z.

Though small on average, the wet component is highly variable, contributing to τ^z significant dynamics that are not present in surface pressure. This explains some of the irregularity of the IGS ZND data relative to surface pressure (Fig. 1, right panel). The effect of water vapor dynamics on

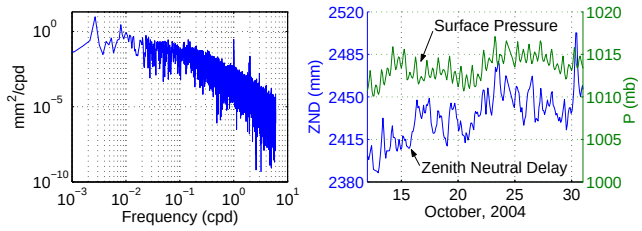

Figure 1. Left panel: Power spectrum of ZND data taken from IGS station BAHR (50.6°E, 26.2°N) for 2000-2005. Abscissa units are cycles per day (cpd). Spectral peaks are visible at harmonics of the solar day and at the lunar tidal frequency. Right panel: Time history of ZND and surface pressure measurements from BAHR. Diurnal and semidiurnal variations are evident in both plots.

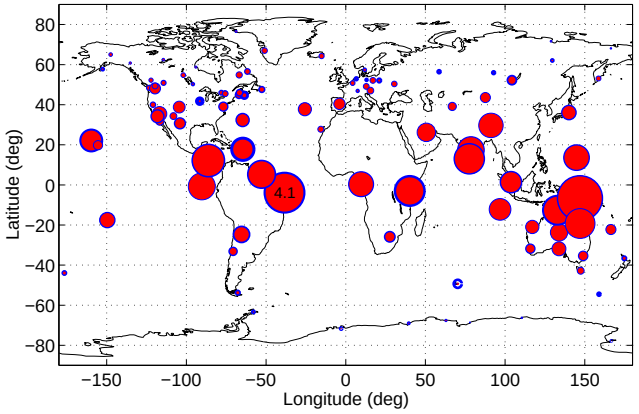

Figure 2. Global distribution of annual mean $S_2(\tilde{\tau}^z)$ amplitude. The amplitude at IGS site FORT (4.1 mm) is labeled for scale. The blue annulus about each dot gives a measure of the $S_2(\tilde{\tau}^z)$ signal-to-noise (SNR) ratio at that site (see AM for details). At SNR = 1, the blue annulus completely covers the red dot.

$S_2(\tau^z)$ has not been well established. *Dai et al.* [2002] detected a ∼0.1-mm semidiurnal variation in GPS-derived precipitable water vapor (PWV) estimates over North America, amounting to a ∼0.7-mm semidiurnal variation in τ_w^z—comparable in amplitude to the semidiurnal variation in τ_h^z. On the basis of this estimate, one would expect τ_w^z to significantly influence the response of τ^z to S_2 forcing. But whereas *Dai et al.* [2002] conclusively demonstrated a large diurnal variation in PWV, the reported semidiurnal variation is much smaller than the rms errors for GPS-derived PWV and was not visible in independent radiosonde and MWR measurements. As will be shown subsequently, the irregularities in $S_2(\tilde{\tau}^z)$ at some IGS sites are consistent with the hypothesis that there exist significant local semidiurnal signals in τ_w^z. However, in general, the $S_2(\tilde{\tau}^z)$ variation is well predicted by its hydrostatic component alone.

This study analyzes the new IGS ZND product (available at ftp://cddis.gsfc.nasa.gov/gps/products/trop_new) for the interval October 2000 to June 2005 and for 100 sites distributed globally as indicated by the dots in Figs. 2 and 3. The new IGS ZND product is based on the precise point positioning technique. It has a higher sampling rate and lower

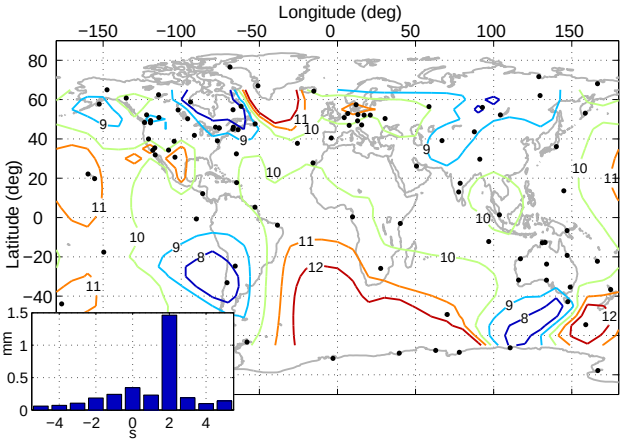

Figure 3. Annual mean $S_2(\tilde{\tau}^z)$ phase isolines. Phase is expressed as local mean solar time at first tidal maximum. Accuracy of the isolines is limited by the sparse spatial resolution of the sites used (black dots). Inset: Global average $S_2(\tilde{\tau}^z)$ wave components.

formal errors than the legacy IGS ZND product [*Byun et al.*, 2005]. Most (79) of the sites are Reference Frame sites, which are subject to strict standards of data quality and continuity. Gaps are common in the data, but at least 2 years of ZND estimates are available for each site. The IGS data are downsampled from 5- to 15-min intervals and the harmonic coefficients a_2 and b_2 of the oscillation at the S_2 frequency are estimated by least squares from the ZND time series for each site. These are used to calculate the mean amplitude A_2 and phase σ_2 of $S_2(\tilde{\tau}^z)$ over the data interval:

$$S_2(\tilde{\tau}^z) = A_2 \sin(2t' + \sigma_2) = a_2 \cos 2t' + b_2 \sin 2t' \quad (3)$$

Here, t' is local mean solar time (LST) in degrees. Zonal harmonic analysis of the harmonic coefficients follows the procedure outlined by *Haurwitz and Cowley* [1973]. First, a_2 and b_2 are interpolated onto a regularly-spaced 5° lat by 10° long grid. Next, the gridded coefficients around each line of latitude θ_i are expanded using a trigonometric series of the longitude λ. This yields a decomposition of S_2 into wave components $S_2(t, \theta_i) = \sum_{s=-\infty}^{\infty} S_2^s(t, \theta_i)$, where s is wave number and t is Universal Time. Predominant among the wave components is the migrating tide S_2^2, which moves westward at the speed of the mean Sun. All zonal wave components with wave numbers $s \neq 2$ are termed nonmigrating wave components; $s = 0$ is a standing wave; wave numbers $s < 0$ move eastward.

3. Observations

Results of the global analysis of $S_2(\tilde{\tau}^z)$ are presented in Figs. 2 and 3. These may be compared with similar plots for $S_2(p)$ reported by *Haurwitz and Cowley* [1973], *Dai and Wang* [1999], and *Ray* [2001]. The data underlying Figs. 2 and 3 are available in tabular format in the auxiliary material (AM).[1]

The large-scale features of the $S_2(\tilde{\tau}^z)$ amplitude distribution, which forgive deficiencies in the spatial resolution of the 100 sites used, correlate well with large-scale features of $S_2(p)$; namely, $S_2(p)$'s characteristic zonal homogeneity and its amplitude increase toward the equator. A comparison of the latitudinal distribution of $S_2(\tilde{\tau}^z)$'s and $S_2(p)$'s

migrating components is presented in the AM, leading to an estimated $S_2^2(\tilde{\tau}^z)/S_2^2(p)$ scale factor of 1.9 mm mb^{-1}—near the scale factor predicted by the hydrostatic approximation. This suggests that, on average, $S_2(\tilde{\tau}^z)$ is dominated by its hydrostatic component.

The $S_2(\tilde{\tau}^z)$ phase distribution exhibits a predominant phase near 150°, corresponding to tidal maximum at 1000 LST. This is consistent with the global average phase for $S_2(p)$, which is 158° (0940 LST). The phase of $S_2(\tilde{\tau}^z)$ is more irregular at middle and low latitudes than that of $S_2(p)$ (irregularity at high latitudes is expected—a result of the increasing dominance of the S_2^0 standing wave toward the poles). This is due in part to systematic errors in ZND and to the short ZND data record, but may also indicate wet component influences on $S_2(\tilde{\tau}^z)$.

The global mean wave components of $S_2(\tilde{\tau}^z)$ (inset of Fig. 3) agree closely with surface pressure data. The migrating wave component, S_2^2, predominates as expected for the S_2 tide. The next largest contribution for both data sources is the standing wave, S_2^0. As a consequence of amplitude and phase irregularities, the non-migrating wave components are more pronounced in the ZND data than in the surface pressure field [e.g., $S_2^2(\tilde{\tau}^z)/S_2^0(\tilde{\tau}^z) \simeq 4$ vs. $S_2^2(p)/S_2^0(p) \simeq 10$].

4. Error Analysis and Discussion

The results of the previous section are encouraging insofar as they suggest that $S_2(\tilde{\tau}^z)$ behaves generally as expected: it is dominated by its hydrostatic component. The 'fingerprint' of the hydrostatic tide in the amplitude and phase data (most striking in the wave component analysis) makes it unlikely that $S_2(\tilde{\tau}^z)$ is caused primarily by variations in EOP, ocean tide loading, or solid earth tides. Each of these has its own unique global phase and amplitude fingerprint, different from that of the $S_2(\tilde{\tau}^z)$ and $S_2(p)$ tides. (For example, the anelastic response of the solid Earth to the solar tide potential causes the maximum solid-earth deformation to occur after local noon, in contrast to the phase shown in Fig. 3.) Similarly, it is unlikely that errors in the final IGS orbit estimates couple into the ZND estimates in such a way as to closely replicate the hydrostatic tide (except in the case of atmospheric pressure loading, which will be discussed subsequently). Nonetheless, incongruities between the global distributions of $S_2(\tilde{\tau}^z)$ and $S_2(p)$ warrant closer examination. It is the purpose of this section to further assess the validity of $S_2(\tilde{\tau}^z)$ by examining its precision and considering likely sources of error.

A tidal determination's precision is calculated by dividing the data record into smaller subrecords that are assumed to be stochastically independent. The mean amplitude and phase of these samples are considered significant if the mean tidal amplitude is at least 3 times greater than the semi-major axis of its 1σ error ellipse [*Chapman and Lindzen*, 1970]. To assess $S_2(\tilde{\tau}^z)$ precision, 13 sites with nearly continuous data records from 2000 to 2005 were chosen for statistical analysis. Of these sites, 9 were equipped with a meteorological (MET) package providing surface pressure measurements, enabling a site-by-site comparison of $S_2(\tilde{\tau}^z)$ and $S_2(p)$ (MET data for site MKEA were taken from the MET package of a nearby telescope). The ZND and surface pressure records are divided into 4 one-year subrecords, each beginning on the same day of the year. From these, a four-sample amplitude and phase standard deviation is computed. The entire 5-year interval is used to evaluate the mean amplitude and phase. Results are reported in Table 1. All the determinations of $S_2(\tilde{\tau}^z)$ are significant except for those corresponding to sites YELL and ALGO, whose high latitudes explain the difficulty in the determination. All the determinations of $S_2(p)$ from MET data are significant. In all comparable cases, the precision of the MET determination is superior to that of ZND. Possible sources of random errors in $S_2(\tilde{\tau}^z)$ are phase range measurement errors and random fluctuations in τ_w^z.

Table 1. ZND and surface pressure (MET) determinations of S_2. Longitude in deg. E, latitude in deg. N, height in m, ZND amplitude in 10^{-2}mm, pressure amplitude in 10^{-2}mb, phase in deg. Error bounds are 1σ values.

Station Data				**ZND**		**MET**	
Site	lon	lat	ht	A_2	σ_2	A_2	σ_2
YELL	246	63	181	27±5	157±29	–	–
POTS	13	52	174	27±6	148±8	32±1	142±2
WTZR	13	49	666	60±9	134±16	36±1	143±1
ALGO	282	46	202	48±14	200±20	–	–
GOLD	243	35	987	149±12	148±3	–	–
JPLM	242	34	424	131±14	84±9	69±1	150±1
MDO1	256	31	2005	111±18	91±8	70±1	154±1
LHAS	91	30	3622	249±19	156±5	106±2	157±1
BAHR	51	26	-17	190±12	162±1	87±1	160±1
KOKB	200	22	1167	224±6	92±2	86±1	164±1
MKEA	205	20	3755	96±10	118±3	83±1	161±1
TOW2	147	-19	87	303±18	154±1	125±2	163±1
HRAO	28	-26	1414	107±16	135±7	–	–

Two features of Table 1 invite further attention. First, phase estimates for sites JPLM, MDO1, KOKB, and MKEA are low compared with MET data. Their phases correspond to tidal maxima at about local solar noon. In each case the good phase precision makes it unlikely that random instrument or meteorological noise is to blame. A glance at Fig. 3 shows that, at mid to low latitudes, such departures from $S_2(p)$'s global mean phase (158° or 0940 LST) are exceptional, indicating site-dependent systematic errors or a significant semidiurnal variation in τ_w^z at these sites. A second anomaly in Table 1 is the sharp decrease in $S_2(\tilde{\tau}^z)$ amplitude from KOKB to MKEA, i.e., from the northwest to the southeast extremes of the Hawaiian archipelago—a short span on the scale of the S_2 tide. No other pair of similarly proximate sites with statistically significant determinations of $S_2(\tilde{\tau}^z)$ manifests such a disparity in amplitude. The disparity is unlikely to be caused by errors in the IGS orbits, the solid earth tide models, the transmitter clock biases, or the EOP models since these errors would be approximately common to both KOKB and MKEA. Furthermore, the MET data indicate that the hydrostatic component of the semidiurnal variation is nearly equivalent at the two sites, despite a large difference in height.

The $S_2(\tilde{\tau}^z)$ amplitude at KOKB is within 14% of the value predicted by the hydrostatic scale factor, but the $S_2(\tilde{\tau}^z)$ amplitude at MKEA is 50% lower than predicted. A close examination of MKEA's ZND frequency spectrum in the neighborhood of S_2 reveals that a considerable fraction of $S_2(\tilde{\tau}^z)$ energy is contained in sidebands resulting from a seasonal modulation. The same sidebands are a smaller fraction of $S_2(\tilde{\tau}^z)$ amplitude at KOKB and a much smaller fraction at LHAS, an inland site on the Tibetan Plateau whose height is nearly that of MKEA. One explanation might be that at MKEA's height the marine-influenced atmosphere produces a seasonally-varying semidiurnal oscillation in τ_w^z.

Atmospheric pressure loading (APL), the slight (mm-scale) deformation of the flexible Earth caused by redistribution of atmospheric mass [*Petrov and Boy*, 2004], is a possible error source for $S_2(\tilde{\tau}^z)$. Because APL is site-dependent it contributes to irregularities in $S_2(\tilde{\tau}^z)$; and because APL is caused by variations in surface pressure it is capable of masquerading as an atmospheric tide. None of the analysis

centers that contribute to the IGS final orbits currently includes APL in its measurement model, nor is it included in the models used to generate the new IGS ZND product.

ZND is sensitive to APL through direct and indirect effects. The direct effect occurs simply because more atmosphere separates a depressed station from a GPS satellite at zenith. This effect is small: a 1-cm (worst-case) depression corresponds to a 0.003-mm increase in τ^z. The indirect effect arises because the site position errors caused by APL couple into satellite orbit and ZND estimates. This effect is larger and more difficult to evaluate because it depends on many factors, including: (1) the spatial extent and amplitude of the pressure anomaly, (2) the spatial distribution of the ground sites, (3) the APL response at each site, (4) the elevation cutoff angle, and (5) the estimation strategy used to determine ZND.

A study of the effects of APL on ZND was carried out by simulation. Realistic GPS satellite orbits and phase range measurements were generated for a globally-distributed set of ground stations. The effects of atmospheric loading were simulated by varying station heights in response to a global model of $S_2(p)$. APL sensitivity at each site was specified by regression coefficients from the International Earth Rotation Service Special Bureau for Loading (available at http://www.sbl.statkart.no). The coefficients were doubled to account for local departures from the inverted barometer assumption used in their calculation. Simulation revealed that APL contamination of ZND estimates amounts to less than 11% of the amplitude of the hydrostatic oscillation in ZND. Simulation details and plots are found in the AM.

A final error source considered here is the ZND mapping function (MF). The IGS currently uses the Niell MF to convert neutral slant delays to zenith delays. *Niell* [1996] showed that radiosonde-derived ("truth") MFs exhibit a diurnal variation at low elevation angles—a consequence of temperature-driven changes in the atmospheric scale height. This variation gives rise to a $\sim 0.1\%$ diurnal error at 5° in the hydrostatic Niell MF because the latter does not account for MF variations on time scales less than one year. If only 5° elevation slant delays were used to estimate ZND, a spurious 1.7-mm diurnal variation in estimated ZND would result. Accounting for the average distribution of elevation angles at each site and the 7° IGS elevation cutoff angle, the effect is reduced to 0.5 mm. A semidiurnal error in ZND caused by the same process can be estimated to be ≤ 0.17 mm (or $\leq 11\%$ of the global average $S_2^2(\tilde{\tau}^z)$ amplitude) by recognizing that the semidiurnal atmospheric temperature variation is at least factor of 3 smaller than the diurnal variation. Improved MFs based on numerical weather models (see *Byun et al.* [2005]) can be expected to reduce these periodic errors in ZND estimates.

5. Conclusion

A strong global correlation with $S_2(p)$ suggests that the semidiurnal variation in IGS ZND data, $S_2(\tilde{\tau}^z)$, is due primarily to the actual semidiurnal variation in ZND, $S_2(\tau^z)$, and not to other geophysical signals or to orbit errors. Atmospheric loading and mapping function errors each contribute less than an estimated 11% of $S_2(\tilde{\tau}^z)$ amplitude. Local incongruities between $S_2(\tilde{\tau}^z)$ and $S_2(p)$ may indicate lingering site-dependent errors or result from a semidiurnal variation in water vapor. These incongruities invite further study.

Acknowledgments. The authors are grateful to Jim Ray and Paul Tregoning for their careful comments. Research at Cornell was supported in part by ONR and NSF.

Notes

1. Auxiliary material is available from ftp://ftp.agu.org/apend/gl/2005GL024207.

References

Byun, S. H., Y. Bar-Sever, and G. Gendt (2005), The new tropospheric product of the International GNSS Service, in *Proc. 2005 ION GNSS Conf.*, Institute of Navigation, Long Beach, CA.

Chapman, S., and R. S. Lindzen (1970), *Atmospheric Tides*, Gordon and Breach, New York.

Dai, A., and J. Wang (1999), Diurnal and semidiurnal tides in global surface pressure fields, *J. Atmos. Sci.*, *56*, 3874–3891.

Dai, A., J. Wang, R. H. Ware, and T. Van Hove (2002), Diurnal variation in water vapor over North America and its implications for sampling errors in radiosonde humidity, *J. Geophys. Res.*, *107*(D10), doi:10.1029/2001JD000642.

Davis, J. L., T. A. Herring, I. I. Shapiro, A. E. E. Rogers, and G. Elgered (1985), Geodesy by radio interferometry: Effects of atmospheric modeling errors on estimates of baseline length, *Radio Sci.*, *20*(6), 1593–1607.

Haurwitz, B., and A. D. Cowley (1973), The diurnal and semidiurnal barometric oscillations, global distribution and annual variation, *Pure Appl. Geophys.*, *102*, 193–222.

Humphreys, T., M. Kelley, and P. Kintner (2004), GPS-based measurement of atmospheric tides, in *Proc. 2004 ION GNSS Conf.*, pp. 864–880, Institute of Navigation, Long Beach, California.

Niell, A. E. (1996), Global mapping functions for the atmosphere delay at radio wavelengths, *J. Geophys. Res.*, *101*, 3227–3246.

Petrov, L., and J. Boy (2004), Study of the atmospheric pressure loading signal in very long baseline interferometry observations, *J. Geophys. Res.*, *109*, B03,405, doi: 10.1029/2003JB002500.

Ray, R. D. (2001), Comparisons of global analyses and station observations of the S_2 barometric tide, *J. of Atmos. and Solar-Terrestrial Phys.*, *63*, 1085–1097.

T. E. Humphreys, Sibley School of Mechanical and Aerospace Engineering, Cornell University, Ithaca, N.Y., 14853 USA. (teh25@cornell.edu)